Genetic background-dependent role of *Egr1* for eyelid development

Jangsuk Oh[a,b], Yujuan Wang[c,1], Shida Chen[c,1], Peng Li[a,b], Ning Du[a,b], Zu-Xi Yu[d], Donna Butcher[e], Tesfay Gebregiorgis[a,b], Erin Strachan[f], Ordan J. Lehmann[f], Brian P. Brooks[g], Chi-Chao Chan[c,2], and Warren J. Leonard[a,b,2]

[a]Laboratory of Molecular Immunology, National Heart, Lung, and Blood Institute, National Institutes of Health, Bethesda, MD 20892; [b]Immunology Center, National Heart, Lung, and Blood Institute, National Institutes of Health, Bethesda, MD 20892; [c]Laboratory of Immunology, National Eye Institute, National Institutes of Health, Bethesda, MD 20892; [d]Pathology Core, National Heart, Lung, and Blood Institute, National Institutes of Health, Bethesda, MD 20892; [e]Pathology/Histotechnology Laboratory, Leidos Biomedical Research, Inc., Frederick, MD 21702; [f]Department of Medical Genetics, University of Alberta, Edmonton AB, Canada T6G 2H7; and [g]Ophthalmic Genetics and Visual Function Branch, National Eye Institute, National Institutes of Health, Bethesda, MD 20892

Contributed by Warren J. Leonard, June 30, 2017 (sent for review May 3, 2017; reviewed by David Fisher and Anjana Rao)

EGR1 is an early growth response zinc finger transcription factor with broad actions, including in differentiation, mitogenesis, tumor suppression, and neuronal plasticity. Here we demonstrate that *Egr1*$^{-/-}$ mice on the C57BL/6 background have normal eyelid development, but back-crossing to BALB/c background for four or five generations resulted in defective eyelid development by day E15.5, at which time EGR1 was expressed in eyelids of WT mice. Defective eyelid formation correlated with profound ocular anomalies evident by postnatal days 1–4, including severe cryptophthalmos, microphthalmia or anophthalmia, retinal dysplasia, keratitis, corneal neovascularization, cataracts, and calcification. The BALB/c albino phenotype-associated *Tyr*^{c} tyrosinase mutation appeared to contribute to the phenotype, because crossing the independent *Tyr*$^{c\text{-}2J}$ allele to *Egr1*$^{-/-}$ C57BL/6 mice also produced ocular abnormalities, albeit less severe than those in *Egr1*$^{-/-}$ BALB/c mice. Thus EGR1, in a genetic background-dependent manner, plays a critical role in mammalian eyelid development and closure, with subsequent impact on ocular integrity.

Egr1 | eyelid development | ocular abnormalities | tyrosinase | genetic background-specific effects

The early growth response (*Egr*) family genes, *Egr1*, *Egr2*, *Egr3*, and *Egr4*, are rapidly induced by cell-surface receptor signaling and regulate gene expression in response to a range of mitogenic signals in multiple cell types (1). Human EGR1, also known as ZIF268, NGFI-A, KROX24, TIS8, and ZENK, was first identified as a regulator of the cell cycle (G0/G1 switch) in peripheral blood lymphocytes (2). Sequence analysis of mouse *Egr1* indicated that it was a DNA-binding protein with three highly conserved Cys_2–His_2 zinc finger domains (3), and *Egr1* was established as a transcription regulator (4) that binds to a 5′-GCG TGG GCG-3′ motif. EGR1 has been suggested to have multiple actions, including in differentiation (5, 6), as a tumor suppressor (7, 8, 9), and as a mediator of neuronal plasticity (10, 11). Moreover, EGR1 is expressed in T cells and thymocytes, with actions promoting positive selection of both $CD4^+$ and $CD8^+$ thymocytes (12) and T-cell activation in part by enhancing IL-2 transcription (13).

While studying the role of EGR family proteins in T-cell biology (14), we unexpectedly observed ocular abnormalities associated with *Egr1* deficiency that depended on the genetic background. No abnormalities were observed in *Egr1*$^{-/-}$ C57BL/6 mice, but as these animals were progressively crossed toward the BALB/c background, we observed profound anomalies in adult and newborn mice, including cryptophthalmos, anophthalmia or severe microphthalmia, retinal dysplasia, keratitis, corneal neovascularization, cataracts, and calcification, indicating the importance of the mouse background and the possibility for strain-specific modifier genes affecting eye development. Interestingly, the phenotype was variable, even within the two eyes in a single mouse, indicating variable penetrance. Importantly, during embryonic development, although early development of the eye was normal in *Egr1*$^{-/-}$ (BALB/c background) mice, these animals exhibited defective eyelid formation and closure, whereas this defect was not observed in *Egr1*$^{-/-}$ C57BL/6 mice. Furthermore, we confirmed EGR1 expression in the developing eyelid by immunohistochemistry. We also show that crossing the *Tyr*$^{c\text{-}2J}$-null allele to *Egr1*$^{-/-}$ C57BL/6 mice results in ocular abnormalities; however, these abnormalities were less severe than those that occur in the *Egr1*$^{-/-}$ BALB/c mice, which naturally contain the *Tyr*^{c} mutation. Overall, our data indicate that *Egr1* deficiency results in abnormal eyelid development and closure in a genetic background-dependent manner, predisposing to a range of ocular abnormalities.

Results

Ocular Anomalies in *Egr1*$^{-/-}$ BALB/c but not *Egr1*$^{-/-}$ C57BL/6 Mice. *Egr1*$^{-/-}$ mice on the C57BL/6 background were backcrossed to the BALB/c background. Although no abnormalities were observed in *Egr1*$^{+/-}$ and *Egr1*$^{-/-}$ C57BL/6 mice (Fig. 1*A*) or in *Egr1*$^{+/+}$ and *Egr1*$^{+/-}$ BALB/c mice after five generations of backcrossing (Fig. 1*B*), substantial abnormalities were observed at the F5 *Egr1*$^{-/-}$ BALB/c generation, including cryptophthalmos (narrow palpebral fissure), microphthalmia (small eye size) and, in some mice, opaque cornea (Fig. 1*C*). Compared with normal mice (Fig. 1*D*), histological

Significance

Eyelid formation begins at approximately day E15.5 in mice. Over the next 24 h, the epidermis of both upper and lower eyelids rapidly grows and merges to cover the cornea. Here, we demonstrate that *Egr1*$^{-/-}$ mice on the C57BL/6 background have normal eyelid development, but back-crossing to BALB/c background for four or five generations resulted in defective eyelid development by embryonic day E15.5. This defective eyelid formation was then further associated with profound ocular anomalies evident by postnatal days 1-4. The BALB/c albino phenotype associated with the *Tyr*^{c} tyrosinase mutation also appeared to contribute to the phenotype. Thus EGR1 in a genetic background-dependent manner plays a critical role in mammalian eyelid development, with subsequent impact on ocular integrity.

Author contributions: J.O., O.J.L., B.P.B., C.-C.C., and W.J.L. designed research; J.O., Y.W., S.C., P.L., N.D., Z.-X.Y., D.B., T.G., and E.S. performed research; J.O., P.L., Z.-X.Y., D.B., O.J.L., B.P.B., C.-C.C., and W.J.L. analyzed data; and J.O., P.L., Z.-X.Y., D.B., O.J.L., B.P.B., C.-C.C., and W.J.L. wrote the paper.

Reviewers: D.F., Massachusetts General Hospital Harvard Medical School; and A.R., Sanford Consortium for Regenerative Medicine and La Jolla Institute for Allergy and Immunology.

The authors declare no conflict of interest.

Data deposition: The sequence reported in this paper has been deposited in the National Center for Biotechnology Information Gene Expression Omnibus database (accession no. GSE100690).

[1]Present address: State Key Laboratory of Ophthalmology, Zhongshan Ophthalmic Center, Sun Yat-Sen University, Guangzhou, Guangdong 510060, China.

[2]To whom correspondence may be addressed. Email: wjl@helix.nih.gov or chanc@nei.nih.gov.

This article contains supporting information online at www.pnas.org/lookup/suppl/doi:10.1073/pnas.1705848114/-/DCSupplemental.

analysis revealed anophthalmia (absence of one or both eyes) (Fig. 1*E*), severe microphthalmia (Fig. 1*F*), retinal dysplasia (Fig. 1*G*), cataracts (Fig. 1 *H* and *I*), keratitis (Fig. 1 *H–J*), corneal neovascularization (Fig. 1 *H–J*), and/or calcification (Fig. 1*H* and Table 1). Interestingly, the severity of defects often varied substantially between the two eyes in the same mouse, indicating variable penetrance of the phenotype even within a single animal.

These results suggested that *Egr1* deficiency conferred these ocular abnormalities on the BALB/c but not the C57BL/6 background, but conceivably a de novo mutation in another gene might have occurred spontaneously during backcrossing. We thus performed a second independent backcross of $Egr1^{-/-}$ C57BL/6 mice to the BALB/c background, and by the F4 generation the $Egr1^{-/-}$ but not $Egr1^{+/-}$ or $Egr1^{+/+}$ mice again showed ocular anomalies similar to those of the first backcross, including anophthalmia (Fig. S1*A*), severe microphthalmia (Fig. S1*B*), retinal folds (Fig. S1*C*), keratitis/corneal neovascularization (Fig. S1*D*), and cataracts (Fig. S1*D* and Table 1). These results confirmed that *Egr1* mutation was indeed responsible for the eye defects on the BALB/c background, underscoring the importance of the genetic background and the possibility of contributions from strain-specific modifier gene(s).

Abnormal Eyelid Formation in $Egr1^{-/-}$ BALB/c Embryos and Ocular Abnormalities After Birth. To determine how early the ocular abnormalities occurred, we next studied 1- to 4-d-old mice. As

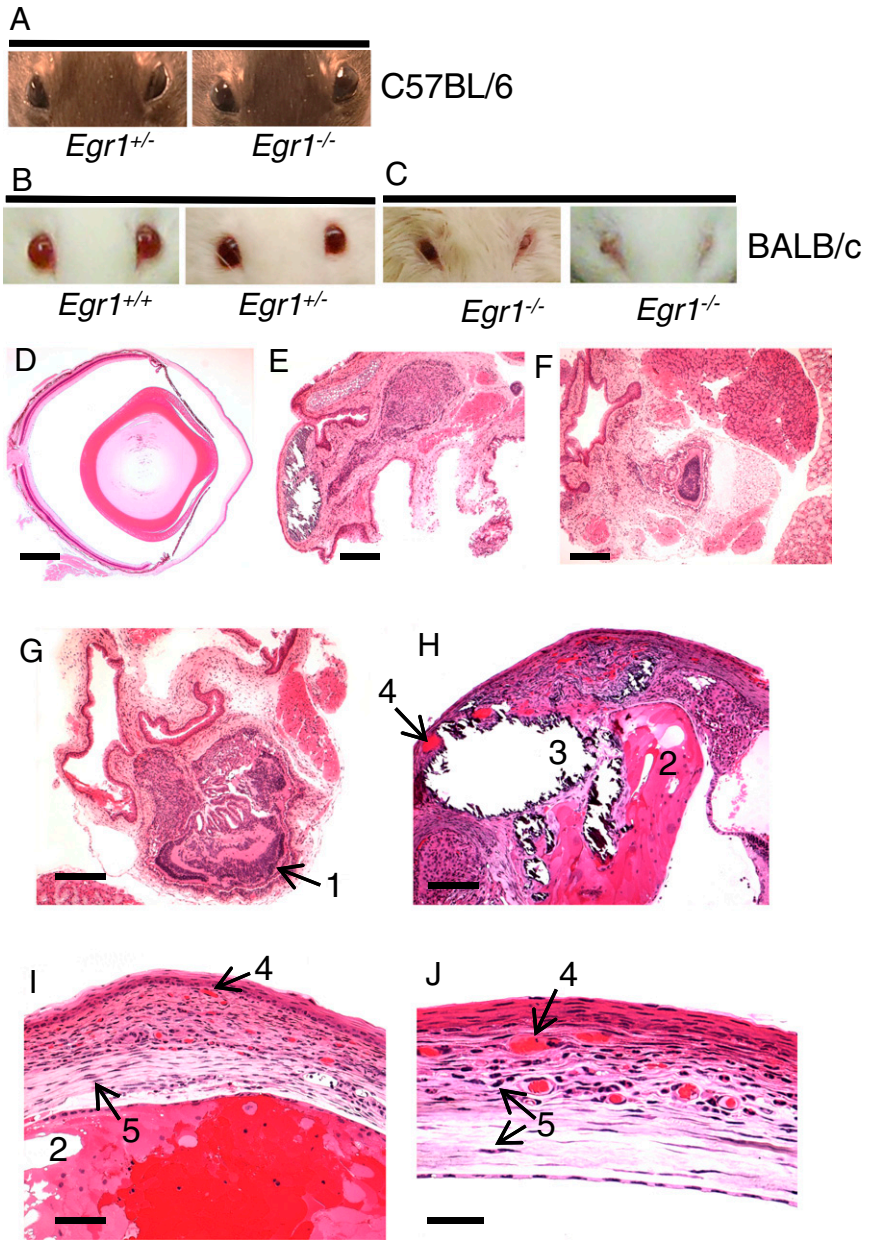

Fig. 1. Defective eye development in adult $Egr1^{-/-}$ BALB/c mice. (*A* and *B*) External view of normal eyes from adult $Egr1^{+/-}$, $Egr1^{-/-}$ C57BL/6 mice (*A*) and adult $Egr1^{+/+}$, $Egr1^{+/-}$BALB/c mice (*B*). (*C*) External view of eyes from adult $Egr1^{-/-}$ BALB/c mice showing abnormal periocular shape and eye size and corneal opacity. (*D*) Histology of adult $Egr1^{+/+}$ BALB/c mice. (*E–G*) Histology of adult $Egr1^{-/-}$ BALB/c adult mice at F5 from the initial backcross, showing anophthalmia (*E*), severe microphthalmia (*F*), and microphthalmia (*G*). (*H–J*) Abnormalities in adult $Egr1^{-/-}$ BALB/c mice. In *G–J*, numbered arrows indicate the following: 1, retinal dysplasia; 2, cataract; 3, calcification; 4, corneal neovascularization; 5, keratitis. (Scale bars: *D*, 800 μm; *E* and *F*, 400 μm; *G* and *H*, 200 μm; *I*, 100 μm; *J*, 50 μm.)

Table 1. Histological analysis of the eyes of adult mice

Mouse ID	*Egr1*	Ocular phenotype
Initial backcross		
NEI 1	KO	Anophthalmia
		Corneal NV, mild keratitis, calcification
NEI 2	KO	Corneal NV, mild keratitis, calcification
		Corneal NV, mild keratitis
NEI 3	KO	Phthisis bulbi
		Loss of eye tissue (remaining on retina tissue)
NEI 5	KO	Anophthalmia
		Corneal NV, mild keratitis
NEI 6	KO	Severe corneal NV, keratitis
		Severe corneal NV, keratitis
NEI 9	KO	Severe microphthalmia, cataracts, corneal NV, mild keratitis, retinal dysplasia
		Microphthalmia, corneal NV, mild keratitis, retinal dysplasia
NEI 18	KO	Anophthalmia
		Severe microphthalmia, corneal NV, mild keratitis, calcification, retinal dysplasia
NEI 21	KO	Severe microphthalmia
		Microphthalmia, retinal dysplasia
NEI 22	KO	Corneal NV, mild keratitis
		Minimal corneal peripheral keratitis
	HT (13)	Both eyes normal
	WT (4)	Both eyes normal
Second backcross		
NEI 30	KO	Both eyes normal
NEI 31	KO	Severe microphthalmia, retinal dysplasia
		Severe microphthalmia
NEI 34	KO	Anophthalmia
		Severe microphthalmia, retinal dysplasia
NEI 35	KO	Corneal NV, mild keratitis, synechiae, vitritis, cataracts
		Corneal NV, mild keratitis, retinal dysplasia
	HT (5)	Both eyes normal
	WT (2)	Both eyes normal

HT, Heterozygote; NV, neovascularization.

expected, eyes from $Egr1^{+/+}$ and $Egr1^{+/-}$ BALB/c mice were normal (Fig. 2*A*); however, histological analysis showed mild corneal neovascularization and keratitis abnormalities in $Egr1^{-/-}$ BALB/c mice at postnatal days 1 and 2 (Fig. 2*B* and Table S1). In one case, an eye was severely malformed (Fig. 2*C*). At postnatal days 3 and 4, $Egr1^{-/-}$ BALB/c mice exhibit a greater severity, including microphthalmia, keratitis, and corneal neovascularization as well as corneal melting and perforation (Fig. 2 *D* and *E*), vitreous hemorrhage (Fig. 2 *E* and *F*), inflammation (Fig. 2 *E*), and retinal detachment (Fig. 2 *E* and *F*) or only residual remnant retina (Fig. 2*G*) (abnormalities are summarized in Table S1). In addition to these abnormalities, a striking finding was that although all $Egr1^{+/+}$ and $Egr1^{+/-}$ BALB/c mice had normal palpebral fissures and thus had normally closed eyelids (Fig. 2 *H* and *I*), 13 of 16 $Egr1^{-/-}$ BALB/c mice had no evidence of eyelid formation and closure at postnatal days 1–4 (Fig. 2*J* and Table S1). Importantly, when eyelids were normally closed in $Egr1^{-/-}$ BALB/c mice, the ocular structure was either normal or had only mild anomalies, compared with mice with unformed eyelids (Table S1), suggesting a causal relationship between the failure of normal eyelid closure and ocular damage.

In mice, eyelid formation is not evident at day E13.5, but the epidermis of both upper and lower eyelids grows rapidly and merges to cover the cornea at approximately day E15.5 over the next 24 h (15–17). To identify when defective eyelid formation occurred, $Egr1^{+/-}$ and $Egr1^{-/-}$ BALB/c embryos were analyzed. At day E16.5, 4 $Egr1^{+/-}$ BALB/c embryos showed epidermis growth, with four of eight embryos having completely merged eyelids and the other four having one eyelid merged (Fig. 3*A*, *Right*) and the other still only partially merged (Fig. 3*A*, *Left*, and Table S2). In contrast, all seven $Egr1^{-/-}$ embryos had defective eyelid formation; fusion was completely defective in four of the seven cases and was partial in the other three (Fig. 3*B* and Table S2). In all E17.5 and E18.5 $Egr1^{+/-}$ BALB/c embryos, both eyelids were completely merged (Fig. 3 *C* and *E*), in marked contrast to the defective eyelid formation in all $Egr1^{-/-}$ BALB/c embryos (Fig. 3 *D* and *F* and Table S2). Despite deformed eyelid formation, the internal ocular structure was relatively normal in all $Egr1^{-/-}$ BALB/c embryos, indicating that the ocular anomalies observed postnatally and in adults, as shown in Fig. 1, occurred later than day E18.5.

***Egr1* Is Expressed in the Eyelid During Embryogenesis.** Because of the defective eyelid formation, we next investigated whether the *Egr1* gene is expressed in the eyelid during embryogenesis. Serial sections of E13.5, E15.5, and E17.5 embryos from C57BL/6 WT mice were stained by immunohistochemistry using an antiserum to EGR1 in the presence (Fig. 4 *A*, *C*, and *E*) or absence (Fig. 4 *B*, *D*, and *F*) of an EGR1-blocking peptide. Although no clear signal was seen in the presence of the blocking peptide, staining of eyes from E13.5 mice demonstrated robust nuclear staining of a subpopulation of mesenchymal cells in the developing eyelids, orbit, and periocular tissues as well as in the epithelia of the developing lens and conjunctival sac (Fig. 4*B*). Strong nuclear EGR1 staining was absent from the neuro-ectoderm–derived presumptive retinal pigment epithelium (RPE) and neural retina (Fig. 4*B*). By E15.5, EGR1 staining was prominent in the surface epithelium covering the now-closed eyelids as well as at the base of the developing cilia (eyelashes) (Fig. 4*D*). At day E17.5, staining was most prominent at the base of hair follicles and in scattered mesenchymal cells (Fig. 4*F*). Similar results were observed when sections from E15.5 embryos from BALB/c WT mice were stained with an antiserum to EGR1 in the presence (Fig. 4*G*) or absence (Fig. 4*H*) of an EGR1-blocking peptide. Prominent EGR1 staining was detected at the base of the developing cilia at the leading edge of the eyelid (Fig. 4*H*). Thus, *Egr1* is indeed expressed in the developing eye, including in the eyelid. Given the expression of EGR1 in the eyelid and the defective eyelid development in *Egr1*-deficient BALB/c background mice, it will be interesting in the future to perform microdissection and subsequent RNA-sequencing (RNA-seq) of eyelid regions in BALB/c WT and KO embryonic mice; this investigation might provide more information related to the genes that are important for eyelid development.

Mutations of *EGR1* Were Not Found in Patients with Coloboma and Multiple Congenital Anomaly Syndrome. Given the abnormalities that we observed in *Egr1*-deficient BALB/c mice, we wondered if *EGR1* deficiency might be associated with congenital ocular abnormalities in humans as well. "Congenital ocular coloboma" refers to defects in which normal tissue in or around the eye is absent from birth and has been reported in 3–11% of blind children worldwide. Typical coloboma—a defect in the inferonasal quadrant of the iris, retina/RPE/choroid and/or optic nerve—is caused by failure of the ventral optic fissure to close during the fifth week of human gestation (18). Rarely, coloboma and posterior staphyloma are reported in isolated cases (19, 20). To evaluate whether *EGR1* might be responsible for a subset of patients with coloboma, 67 unrelated patients with this disease were analyzed, but no mutations were identified in the *EGR1* coding regions or adjacent intronic regions, indicating that mutations in *EGR1* do not explain the occurrence of coloboma in these patients. We also screened 88 multiple congenital anomaly (MCA) patients available to us for *EGR1* mutations and detected a heterozygous variant involving

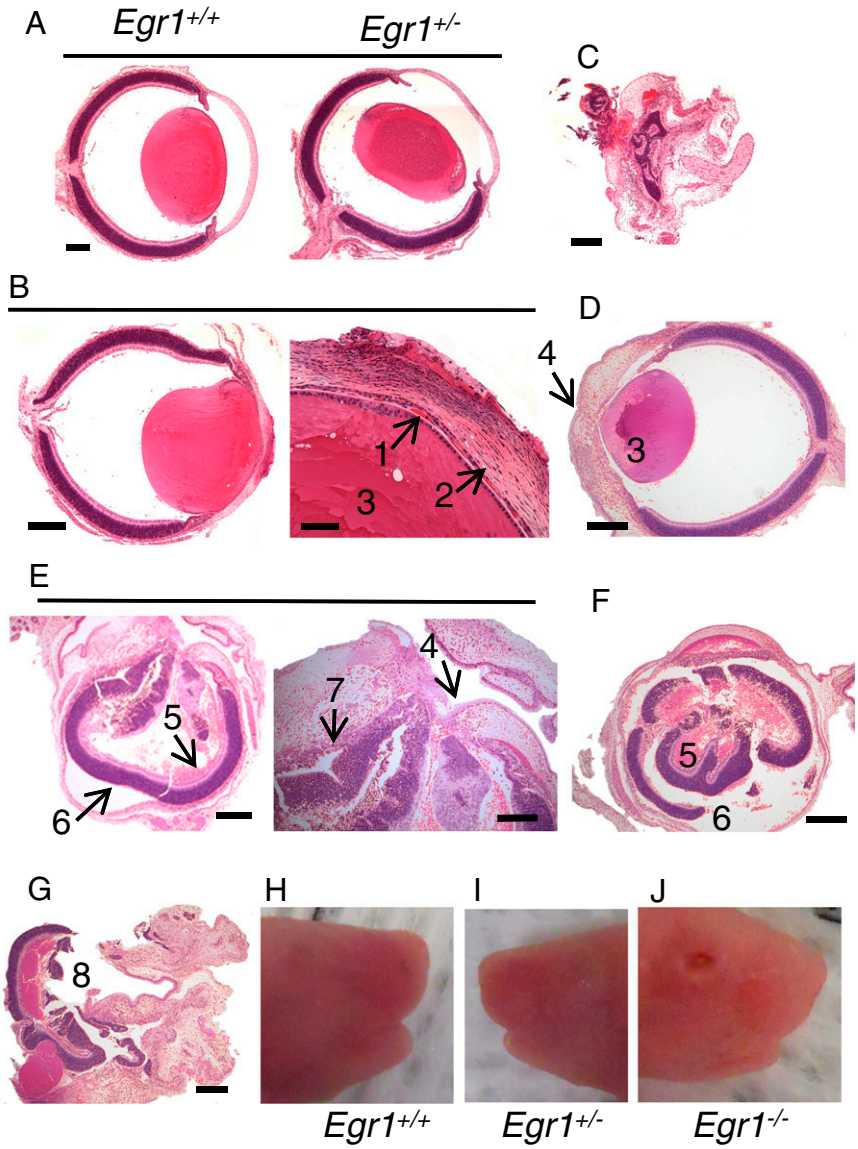

Fig. 2. Abnormal ocular development in postnatal *Egr1*$^{-/-}$ BALB/c mice. (*A*–*G*) Histology of eyes from newborn *Egr1*$^{+/-}$ mice (*A*), *Egr1*$^{-/-}$ mice at postnatal day 1 (*B*) and 2 (*C*), and from *Egr1*$^{-/-}$ mice at postnatal days 3 and 4 (*D*–*G*). In *B* and *D*–*G*, numbered arrows refer to the following: 1, mild corneal neovascularization; 2, mild keratitis; 3, cataracts; 4, corneal perforation; 5, vitreous hemorrhage; 6, retinal detachment; 7, inflammation; 8, residual remnant retina. (*H*–*J*) Eyelids of newborn *Egr1*$^{+/+}$ (*H*) and *Egr1*$^{+/-}$ (*I*) mice are formed, whereas those of *Egr1*$^{-/-}$ mice are not formed, and eyes appear open (*J*). [Scale bars: *A*, *B* (*Left*), and *D*, 800 μm; *C*, 400 μm; *E* (*Left*), *F*, and *G*, 200 μm; *B* (*Right*) and *E* (*Right*), 100 μm.]

nt1600 (C to T), P443L, in one patient. Although this variant has not been recorded in the Ensembl database, heterozygosity suggests that this change is unlikely to be responsible for the defects in this patient.

Identification of Differentially Expressed Genes in *Egr1*$^{-/-}$ BALB/c Mice. A common abnormality in the *Egr1*$^{-/-}$ BALB/c mice was corneal neovascularization. Previously, it was reported that the proinflammatory cytokine IL-1β can induce neovascularization in both C57BL/6 and BALB/c mice (21). We thus measured ocular *Il1b* mRNA levels and found the levels were increased in adult *Egr1*$^{-/-}$ BALB/c mice but not in *Egr1*$^{+/+}$ BALB/c, *Egr1*$^{+/+}$ C57BL/6, or *Egr1*$^{-/-}$ C57BL/6 mice (Fig. 5*A*). Similarly, *Il1b* mRNA was increased in the eyes of newborn *Egr1*$^{-/-}$ BALB/c mice but not in *Egr1*$^{+/+}$ BALB/c or *Egr1*$^{+/-}$ BALB/c mice (Fig. 5*B*), suggesting that IL-1β may be involved in the development of ocular anomalies in *Egr1*$^{-/-}$ BALB/c mice. We therefore backcrossed C57BL/6 mice homozygous for the *Il1r*^{tm1Imx}-targeted mutation, which prevents responsiveness to IL-1, to BALB/c for five generations and then crossed these mice to F5 *Egr1*$^{-/-}$ BALB/c mice to generate double-KO mice. As expected, most (six of seven) *Egr1*$^{-/-}$ BALB/c mutant mice had defects in one or both eyes, but all four *Il1r*^{tm1Imx}*Egr1*$^{-/-}$ BALB/c double-KO mice also had defects related to one or both eyes (Table S3), indicating that disease still progressed even when IL-1β could not function, as is consistent with contributions by other cytokines or growth factors.

To identify other genes that potentially contribute to the ocular phenotype, RNA-seq was performed with RNA from eyes from adult *Egr1*$^{-/-}$ BALB/c mice (see Dataset S1A for the complete RNA-seq data). RNA-seq results confirmed higher *Il1b* expression in *Egr1*$^{-/-}$ BALB/c mice than in WT mice. In addition, there was increased expression of cytoskeleton genes, including the *Krt1*, *Krt16*, *Lor*, *Sprr* family, and *Lce* family genes, which are involved in the process of cornification in which an epidermal barrier is formed

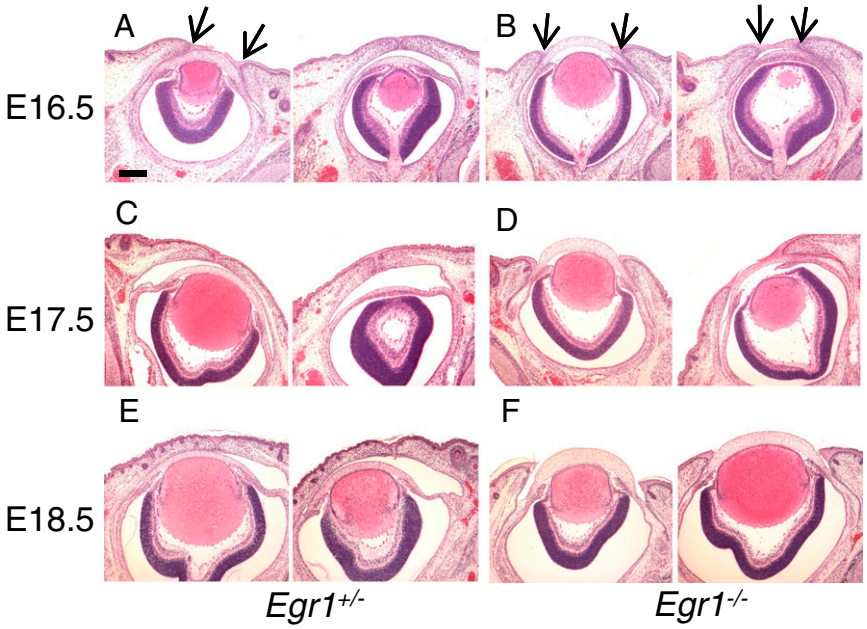

Fig. 3. Eyelid formation in embryos. (*A*, *C*, *E*) *Egr1*$^{+/-}$ BALB/c mice. (*B*, *D*, *F*) *Egr1*$^{-/-}$ BALB/c mice. Two embryos of each indicated genotype are shown at days E16.5 (*A* and *B*), E17.5 (*C* and *D*), and E18.5 (*E* and *F*). The arrows in *A* and *B* indicate areas of eyelid merging or defects therein. (Scale bars: *A*–*F*, 800 μm.)

in stratified squamous epithelial tissue. We also identified increased expression of several kallikrein genes that are involved in the regulation of blood pressure and activation of inflammation. Interestingly, the expression of γ-crystallin genes, *Cryga* and *Cryge*, was significantly lower in *Egr1*$^{-/-}$ BALB/c mice. Crystallins are the main structural proteins of the vertebrate ocular lens, and their appropriate arrangement is critical for lens transparency, with mutations in the *Cryg* genes leading mainly to lens opacification and cataracts (22, 23).

Because we found that internal ocular anomalies occurred after birth, we also performed RNA-seq analyses using eyes from newborn *Egr1*$^{-/-}$ BALB/c mice, revealing increased expression of some of the genes identified in adult mice (see Dataset S1B for the complete RNA-seq data, comparing gene expression in "open" vs. "closed" eyes). In addition to cytoskeleton genes related to cornification, many more keratin genes are highly expressed in *Egr1*$^{-/-}$ BALB/c mice, suggesting keratinization at an early age. In one *Egr1*$^{-/-}$ BALB/c mouse, the expression of many crystallin and lens protein genes was strikingly decreased, possibly explaining why *Egr1*$^{-/-}$ BALB/c mice often develop cataracts.

Because in some *Egr1*$^{-/-}$ BALB/c mice, one eye had normally formed eyelids and a relatively normal ocular structure, whereas the other eye had unmerged eyelids and malformed ocular structure, we performed RNA-seq using RNA from each eye of three 3-d-old *Egr1*$^{-/-}$ mice with unmerged eyelids and from *Egr1*$^{+/-}$ littermate controls. A multidimensional scaling (MDS) plot shows that gene-expression profiles in eyes from *Egr1*$^{-/-}$ mice with unmerged eyelids (eyes that appeared open) were very different from those in eyes from either *Egr1*$^{+/-}$ or *Egr1*$^{-/-}$ mice in which the eyelids formed normally (see Fig. 5*C* and Dataset S2 for the complete RNA-seq data), suggesting that normally closed eyelids prevented ocular anomalies. To identify genomewide targets of EGR1-regulated genes that are important for eye development, differentiation, and function, we analyzed differential gene expression in eyes from mice without or with eyelid closure. We identified 854 and 37 genes that were significantly up- or down-regulated [fold change (FC) >2, $P < 0.05$], respectively, in eyes with defective eyelid closure (Fig. 5*D*). We identified the top 50 most differentially expressed genes, displayed by heat map (Fig. 5*E*; sorted by *P* value) and volcano plot (Fig. 5*F*). Very interestingly, *Sprr1a* (24), *Krt16* (25), and *Il1b*, which previously had been shown to be involved in the development of ocular disease, were highly up-regulated in eyes without eyelids (Fig. 5*G*). Our data overall suggest that the differences in gene expression are secondary to the failure of eyelid formation rather than directly caused by the absence of *Egr1*.

The Role of the *Tyr* Gene in the Ocular Abnormalities. A major difference between C57BL/6 (black) and BALB/c (albino) mice is eye and skin pigmentation. Interestingly, the enzyme tyrosinase, which catalyzes the first two steps of melanin biosynthesis, was previously identified as a modifier of the trabecular meshwork phenotype in a mouse model of human primary congenital glaucoma in which the presence of the homozygous *Tyr*$^{c\text{-}2J}$ allele conferred much more severe developmental defects to *Cyp1b*$^{-/-}$ mice (26). Because homozygous *Tyr*$^{c\text{-}2J}$ mice are on a C57BL/6 background but are phenotypically indistinguishable from BALB/c mice, which harbor the mutant *Tyr*^{c} allele, we investigated whether the *Tyr* gene might contribute to the eyelid abnormalities we observed by crossing *Egr1*$^{-/-}$ C57BL/6 mice to *Tyr*$^{c\text{-}2J}$ homozygous mice. Strikingly, although all pigmented *Egr1*$^{-/-}$ C57BL/6 mice had normal eyes (Fig. 6*A*), 7 of 12 albino *Tyr*$^{c\text{-}2J}$ homozygous *Egr1*$^{-/-}$ C57BL/6 mice developed ocular anomalies. These abnormalities tended to be milder than those in the BALB/c background, with keratitis, corneal neovascularization (Fig. 6*B*), cataracts, anterior synechiae, retinal dysplasia, anterior segment angle defect, and persistent hyperplastic primary vitreous (PHPV) (Fig. 6 *C* and *D* and Table S4), and two albino *Egr1*$^{-/-}$ C57BL/6 mice exhibited full-thickness corneal defects with invasion of epithelium (Fig. 6*C*) as well as staphyloma (Fig. 6*D*). We did not observe staphyloma in any *Egr1*$^{-/-}$ BALB/c mice. Thus, although the *Tyr*$^{c\text{-}2J}$ homozygous mutation increased ocular abnormalities in *Egr1*$^{-/-}$ C57BL/6 mice, the phenotype was less severe than and was somewhat different from that observed in *Egr1*$^{-/-}$ BALB/c mice, indicating that additional modifier gene(s) may contribute to the ocular phenotype of *Egr1*$^{-/-}$ BALB/c mice.

Discussion

The vertebrate eye is a complex structure composed of three major unique tissues, the cornea, the lens, and the retina, the development of which involve highly organized and complex cascades of multiple transcription factors and signals. Mutations in key genes

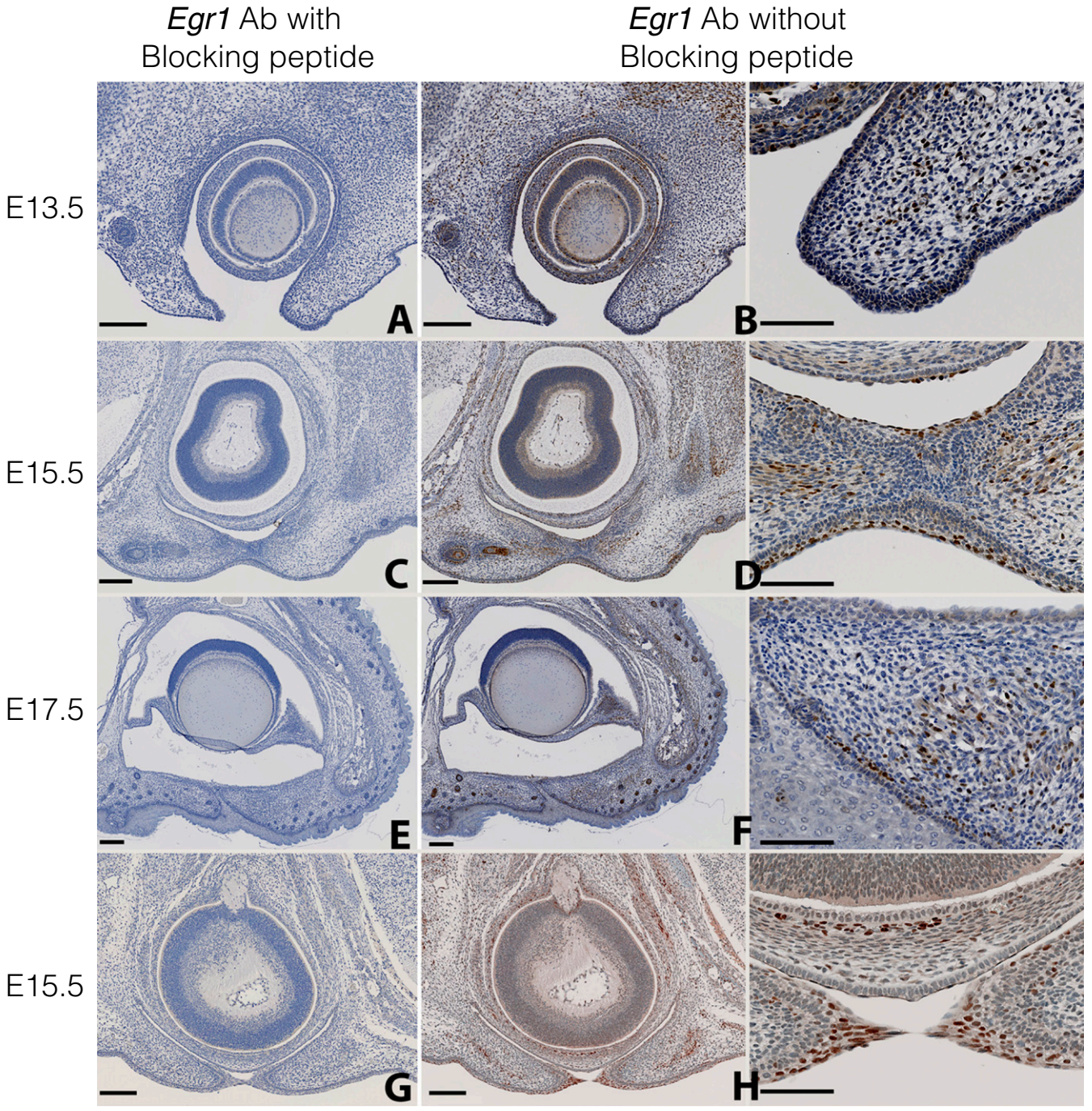

Fig. 4. Immunohistochemistry of *Egr1* during embryogenesis. Two embryos of C57BL/6 WT mice at days E13.5 (*A* and *B*), E15.5 (*C* and *D*), and E17.5 (*E* and *F*) and of BALB/c WT mice at day E15.5 (*G* and *H*). *A*, *C*, *E*, and *G* show controls stained with the *Egr1* Ab-blocking peptide mix, and *B*, *D*, *F*, and *H* show staining with the *Egr1* antibody. In *B*, *D*, *F*, and *H*, *Left* are the same magnification as in panels *A*, *C*, *E*, and *F*, respectively, whereas *B*, *D*, *F*, and *H*, *Right* show a higher-magnification view of the relevant region of the left panel. [Scale bars: *A*, *B* (*Left*), *C*, *D* (*Left*), *E*, *F* (*Left*), *G*, and *H* (*Left*), 200 μm; *B* (*Right*), *D* (*Right*), *F* (*Right*), and *H* (*Right*), 100 μm.]

cause a number of congenital eye disorders (27). Previous genetic studies in zebrafish, flies, chicken, mice, and humans have revealed many key steps in eye development (reviewed in refs, 27 and 28).

We report here that *Egr1* mutation in the BALB/c background mice leads to variable ocular anomalies associated with defective eyelid formation. Interestingly, in chicks exposed to positive or negative lenses to induce defocus, *Egr1* expression was increased with positive lenses that suppress ocular elongation and decreased with negative lenses that enhance ocular elongation (29, 30). Consistent with this observation, $Egr1^{-/-}$ mice have longer eyes with a relative myopic shift in refraction, with additional minor effects on anterior chamber depth and corneal radius of curvature (31); however, analysis of humans with myopia did not reveal EGR1 abnormalities (32). *Egr1* contributes to oculogenesis in zebrafish (33), with arrested retinal and lenticular development and smaller lenses when morpholino oligonucleotides targeting *Egr1* mRNA were microinjected into zebrafish embryos. Our current study identifies EGR1 defects associated with eyelid

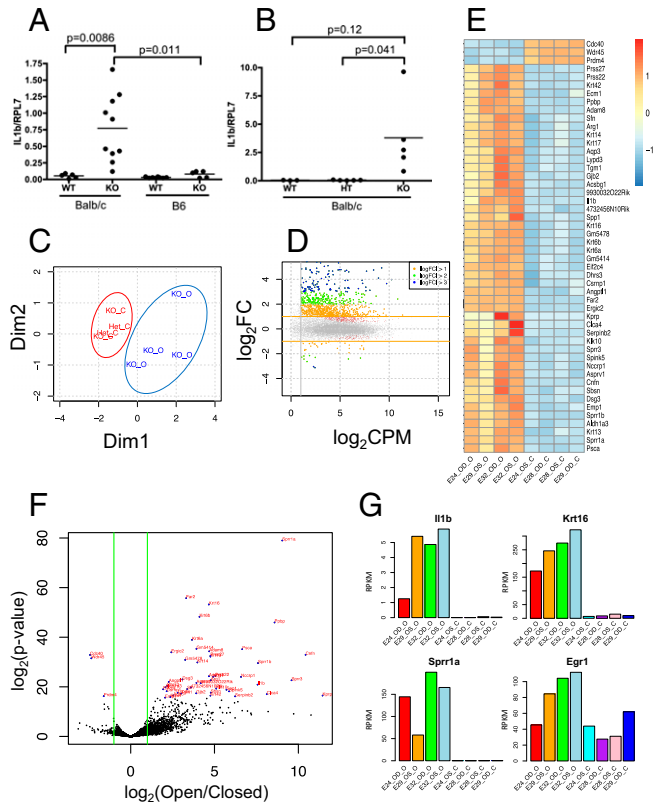

Fig. 5. Gene-expression profiles in eyes from *Egr1*$^{+/-}$ and *Egr1*$^{-/-}$ BALB/c mice. (*A*) *Il1b* mRNA expression is significantly increased in adult *Egr1*$^{-/-}$ BALB/c but not in *Egr1*$^{-/-}$C57BL/6 mice. (*B*) *Il1b* mRNA is increased in *Egr1*$^{-/-}$ BALB/c newborn mice. RNA was normalized relative to the expression of *Rpl7*. Comparison between samples was done by the Student's *t* test. (*C*–*G*) Gene-expression profiles in eyes from *Egr1*$^{+/-}$ and *Egr1*$^{-/-}$ BALB/c mice at postnatal day 3. (*C*) MDS analysis for individual samples from eyes from *Egr1*$^{+/-}$ and *Egr1*$^{-/-}$ mice with formed eyelids (indicated by a "C" for closed) vs. *Egr1*$^{-/-}$ mice without eyelid formation (indicated by an "O" for open). Differences in dimension 1 (Dim1, *x* axis) indicates greater differences in samples than do differences in dimension 2 (Dim 2, *y* axis). (*D*) 2D scatter plot shows expressed genes. Genes highlighted in blue, green, and orange indicate differentially expressed genes with |log2FC|>3, (|log2FC|>2), and |log2FC|>1, respectively. "log2FC" refers to the log (base 2) of the fold change of mRNA expression in eyes with unformed eyelids vs. eyes with formed eyelids. log2CPM, log base 2 of counts per million. (*E*) Heat map of the top 50 differentially expressed genes. The expression matrix on rows is normalized by z-scores, and the colors of the heat map are mapped linearly to the z-scores. Samples ending in "O" were from open eyes of a given embryo; those ending in "C" were from closed eyes. (*F*) Volcano plot showing the top 50 differentially expressed genes. The *x* axis represents the log2FC between eyes from *Egr1*$^{-/-}$ mice with unformed eyelids (open) vs. *Egr1*$^{-/-}$ *or Egr1*$^{+/-}$ mice with fused eyelids (closed), and the *y* axis shows the −log10 of the *P* value. (*G*) Bar plots show the expression of *Il1b*, *Krt16*, *Sprr1a*, and *Egr1*. OD, right eye; OS, left eye. E24, E28, E29, and E32 are the originally designations for these embryos based on when they were collected. RPKM, reads per kilobase of transcript per million mapped reads.

formation; the overall ocular anomalies caused by the absence of eyelid we have observed in this study are more severe, including cryptophthalmos, anophthalmia, microphthalmia, retinal dysplasia, keratitis, corneal neovascularization, and cataracts.

Strikingly, we found a fairly normal internal morphology of the eye in E14.5–E18.5 *Egr1*$^{-/-}$ BALB/c embryos, but eyelid abnormalities were profound. Although both eyelids formed normally and merged in all *Egr1*$^{+/-}$ BALB/c embryos at E17.5–E18.5, most eyelids were still underdeveloped in littermate *Egr1*$^{-/-}$ BALB/c embryos. That the ocular structure was either normal or only mildly malformed when eyelids formed (Table S1), compared with their being open in *Egr1*$^{-/-}$ BALB/c neonatal mice, suggests that open eyelids allowed exposure of the cornea to drying, infection, or other damage, resulting in corneal neovascularization, keratitis, and even perforation, as well as other additional ocular anomalies. This interpretation is further supported by the observation that ocular anomalies were much severe at postnatal days 3 and 4 than at postnatal days 1 and 2 (Table S1).

During ocular development, each layer of the eye is progressively induced by another; retina is formed first; retina formation induces lens development, which in turn induces cornea formation, which finally induces proper eyelid formation. Thus, eyelid defects can be secondary to ocular maldevelopment. However, when we compared the internal structure of eyes from E14.5 *Egr1*$^{+/-}$ BALB/c and *Egr1*$^{-/-}$ BALB/c embryos, no abnormality was found (Fig. S2). This result suggests that the eyelid defect reported here is not secondary to ocular maldevelopment, although we cannot exclude the possibility that a separate, primarily ocular role of EGR1 contributes to the postnatal microphthalmia and is coincident with defective eyelid malformation. Interestingly, MEK kinase 1 (MEKK1), which is required for JNK activation by TGF-β, was previously shown to result in defective embryonic eyelid closure (34). Moreover, TGF-β can stimulate the expression of EGR1, and this TGF-β–induced increase in EGR1 is blocked by a MEK1 inhibitor (35). Our findings therefore may help clarify these prior observations further, although the genetic background-specific phenotype we observe is distinctive, given that the *Mekk1*-deficient mice had been crossed to C57BL/6 mice (34).

Patients with coloboma and with MCA have a different array of ocular problems. We performed sequence analysis of *EGR1* in 67 patients with coloboma and 88 patients with MCA and found no mutations, indicating that EGR1 mutations in humans are not responsible for these diseases. Interestingly, no pathologic mutations have been reported in the *EGR1* gene in humans, although

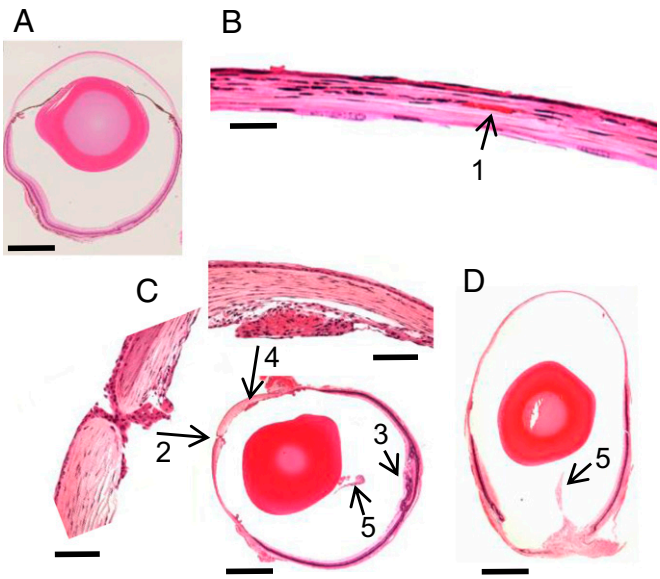

Fig. 6. Histology of *Egr1*$^{-/-}$, *Tyr*$^{c\text{-}2J/c\text{-}2J}$ C57BL/6 mice. (*A*) Normal structure of eyes from *Egr1*$^{-/-}$, *Tyr*$^{+/c\text{-}2J}$ C57BL/6 adult mice. (*B*–*D*) Abnormalities in *Egr1*$^{-/-}$, *Tyr* $^{c\text{-}2J/c\text{-}2J}$ C57BL/6 adult mice. (*B*) Mild corneal neovascularization (1). (*C*) Poor corneal closure with epithelial ingrowth (2), retinal dysplasia (3), anterior angle dysplasia and ciliary body hypoplasia (4), and PHPV (5). The left and upper panels are higher- magnification views of the indicated areas. (*D*) Staphyloma, posterior coloboma, and PHPV. [Scale bars: *A*, *C* (*Bottom*), and *D*, 800 μm; *B*, 50 μm; *C* (*Left* and *Top*), 100 μm.]

EGR1 expression has been associated with tumorigenesis in various cancers (4).

Previous reports suggested that the inflammatory cytokine IL-1β induces neovascularization in the mouse cornea (21). When we measured the ocular *Il1b* mRNA levels, there was a large increase only in $Egr1^{-/-}$ BALB/c adult and newborn mice, but not in $Egr1^{+/+}$ BALB/c and $Egr1^{-/-}$ C57BL/6 mice (Fig. 5 *A* and *B*). This observation suggests that IL-1β may be involved in the keratitis and corneal neovascularization occurred in $Egr1^{-/-}$ BALB/c mice and possibly in the further development of other ocular anomalies. However, when we generated $Il1r^{tm1Imx}Egr1^{-/-}$ BALB/c double-KO mice, they also exhibited ocular malformation, suggesting that IL-1β is not a modifier in this case but rather that the increased level of IL-1β expression could be secondary to keratitis and ocular inflammation in $Egr1^{+/+}$ BALB/c mice.

RNA-seq revealed differential expression of several cytoskeleton genes related to cornification, especially some of the keratin genes, which may lead to the increased keratinization we observed. In one mouse, we also observed the differential expression of many other genes, including crystallins, which are involved in cataract formation; the expression of *Bfsp1* (filesin) and *Bfsp2* (phakinin) mRNA also was decreased significantly in this mouse. These genes encode lens cell-specific intermediate filaments that are believed to promote the maintenance of lens transparency (36). In addition, the expression of other lens proteins, including *Mip*, *Lim2*, *Gja3*, and *Lenep*, were significantly lower in this particular mouse. A mutation in the *Mip* gene causes the Fraser cataract phenotype in mice (37). MIP is the most abundant (50–60%) intrinsic membrane protein of the lens fiber (38). A mutation in the mouse *Lim2* gene causes total opacity of the lens with a dense cataract combined with microphthalmia. In *Lim2*-mutant mice, the lens capsule ruptures posteriorly with lens material leaking into the vitreous chamber (39). *Gja3* gene-targeted null mice developed lens nuclear cataracts shortly after birth (40). Taken together, down-regulation of these genes may result in the formation of the cataracts frequently observed in $Egr1^{-/-}$ BALB/c mice. It has been reported previously that kittens and puppies open their eyelids at about 10–14 d of age and that premature opening results in corneal desiccation, keratitis, corneal ulceration, and conjunctivitis, because several weeks are required for tear production to reach adequate levels. If these consequences are not treated (e.g., with a topical lubricating ophthalmic ointment), corneal perforation and endophthalmitis may occur (41). Such observations support our model proposing that the ocular defects we observed are secondary to defective eyelid closure.

Remarkably, we observed ocular abnormalities in $Egr1^{-/-}$ mice on the BALB/c but not C57BL/6 background, suggesting strain-specific modifier genes. One major difference between the two stains is pigmentation, which seemed potentially germane given that melanin pigment is produced in the uveal melanocytes and retinal pigment epithelium of the eye as well as by neural crest-derived melanocytes found in skin (42). The albino phenotype in BALB/c mice results from deficient activity of tyrosinase, which catalyzes the first two steps of melanin biosynthesis. A naturally arising G-to-C (Tyr^{c}) transversion, resulting in a Ser-to-Cys mutation at codon 103, results in a loss of tyrosinase activity (42). Albino (homozygous for the $Tyr^{c\text{-}2J}$ allele) $Cyp1b^{-/-}$ mice have extensive developmental defects compared with pigmented $Cyp1b^{-/-}$ mice; these defects identify tyrosinase as a modifier in a model of developmental glaucoma (26). The $Tyr^{c\text{-}2J}$ mutation, a G-to-T transversion resulting in an Arg-to-Leu substitution at codon 77, occurred spontaneously in C57BL/6 mice, and homozygous $Tyr^{c\text{-}2J}$ mice are phenotypically indistinguishable from BALB/c (Tyr^{c}) mice. When we examined the $Tyr^{c\text{-}2J}$ homozygous (albino) $Egr1^{-/-}$ C57BL/6 mice, we found relatively mild defects (Table S4), although one $Tyr^{c\text{-}2J}$ homozygous (albino) $Egr1^{-/-}$ C57BL/6 mouse exhibited a full-thickness defect in the cornea (Fig. 6*C*). Thus, although the $Tyr^{c\text{-}2J}$ mutation confers a susceptibility to ocular abnormalities in $Egr1^{-/-}$ C57BL/6 mice, these abnormalities are much less severe than those observed in $Egr1^{-/-}$ BALB/c mice, and there was no obvious defect in eyelid formation because the animals we examined were born with closed eyelids. In the future, it will be interesting to determine if the severity of the ocular defect is diminished if one analyzes $Egr1^{-/-}$ BALB/c background mice that no longer carry an albino phenotype.

In summary, we here report striking defects in eyelid formation in $Egr1^{-/-}$ mice on the BALB/c but not the C57BL/6 background, with profound ocular defects resulting from these eyelid defects. Our data implicate *Tyr* as one modifier gene but also suggest the existence of additional modifier gene(s) to explain the strain specific-defects, an area for future investigation.

Materials and Methods

Mice. All animal experiments used protocols approved by the National Heart, Lung, and Blood Institute (NHLBI) Animal Use and Care Committee and followed NIH guidelines for humane animal use. $Egr1^{-/-}$ C57BL/6 mice (43) were from the Jackson Laboratory (Stock no. 012924) and genotyping was performed by PCR with primer sequences from the Jackson Laboratory. The mice were backcrossed to BALB/c mice from the Jackson Laboratory for five generations in the initial backcross or for four generations in the second backcross. Homozygous $Tyr^{c\text{-}2J}$ mice (stock number 58; Jackson Laboratory) were crossed to $Egr1^{-/-}$ C57BL/6 mice. Mice homozygous for the $Il1r^{tm1Imx}$-targeted mutation (stock number 3245; Jackson Laboratory) were backcrossed to BALB/c mice for five generations and then were crossed with F5 $Egr1^{-/-}$ BALB/c mice to generate double-KO mice. Adult mice were examined between 6 and 21 wk of age.

Ocular Examination. Eyelids, conjunctivae, corneas, anterior chambers, irises, lenses, and retinas of embryonic, neonatal, and adult mice were examined under a slit-lamp biomicroscope (Space Coast Laser, Inc.) and/or dissecting microscope.

Histology and Immunohistochemistry. Eyes including the eyelids from neonatal and adult mice were enucleated and fixed in 4% glutaraldehyde for 30 min, in 10% formalin for >24 h, embedded in methacrylate, and sectioned via a vertical pupillary–optic nerve plane. Mouse embryos were decapitated, and whole heads were fixed in 10% formalin for >24 h, embedded in methacrylate, and sectioned in the coronal plane through the pupillary–optic nerve axis. Specimens that contained bone (osseous tissue) were deparaffinized in xylenes and rehydrated through graded ethanols. Each eye was cut and stained with H&E. For EGR1 staining, C57BL/6 mouse embryos were fixed in 10% buffered formalin, embedded in paraffin, and serial sections (5 μm thick) were cut for histology and immunohistochemistry. Endogenous peroxidase was blocked with 3% H_2O_2. Sections then were subjected to antigen retrieval using a citrate buffer (BioGenex) for 10 min at 100 °C. Following a 5% normal goat serum block, three sets of slides were incubated overnight at 4 °C with (*i*) *Egr1* Ab (rabbit mAb) (no. 4153; Cell Signaling Technology) at 1:100, (*ii*) *Egr1* Ab/blocking peptide (no. 1015; Cell Signaling Technology) mix (1:2 by volume), and (*iii*) rabbit monoclonal IgG isotype control reagent (no. 3900; Cell Signaling Technology). Slides were rinsed, and biotinylated goat anti-rabbit IgG (Vector Labs) that had been diluted 1:100 in TBS-Tween was applied for 30 min. After rinsing in TBS-Tween, Avidin Biotin Complex (Peroxidase ABC kit; Vector Labs) was applied to the slides for 30 min. Localization was visualized by incubation in diaminobenzidine (DAB) substrate for 5 min. Sections were counterstained with H&E, and then coverslips were added.

RNA Isolation and RT-PCR Analysis. Eyes were enucleated and placed into Eppendorf tubes filled with RNAlater (Thermo Fisher), and total RNA was extracted using the RNeasy Mini Kit (Qiagen). The first strand was reverse-transcribed using the Omniscript Reverse Transcription Kit (Qiagen) and random primers. Real-time quantitative PCR was performed on a 7900HT Real-time PCR system (Applied Biosystems) using real-time primers and TaqMan probes for *Il1b* from Applied Biosystems. Expression was normalized to that of *Rpl7*.

RNA-Seq Analysis. Poly(A)$^+$ RNA was selected twice from total RNA using Dynal oligo magnetic beads (Invitrogen). Double-stranded cDNA was synthesized using SuperScript (Invitrogen) and fragmented using Bioruptor (Diagenode). Adaptors (Illumina) were ligated to the dsDNA using T4 DNA ligase (New England Biolabs) after end repair using the End-It Kit (Epicentre) and dA addition. Libraries were size-selected for 250- to 400-bp fragments, purified using 2% E-Gel (Invitrogen), and amplified for 18 cycles by PCR with PE 1.0 and PE 2.0 primers (Illumina) and Phusion High Fidelity PCR Master

Mix (New England Biolabs). PCR products were sequenced on a Solexa 2G Genome Analyzer (Illumina). DNA sequence reads were mapped to the mouse genome [RefSeq gene database using the mm8 revision from the University of California, Santa Cruz (UCSC) genome browser]; 24,769 genes were used for RNA-seq analysis. RNA-seq data have been deposited in the Gene Expression Omnibus (National Center for Biotechnology Information).

DNA Sequencing of the Human EGR1 Gene. The *EGR1* gene was amplified by PCR with the following primers: for exon 1, forward primer 5′-CCGGTCCTGCCATATTAGG and reverse primer 5′-GGCAAGGCAAGTCTTACTGG; for exons 2–3, forward primer 5′-GCCACTGGTGCGGGTCCAGGA and reverse primer 5′-CATGGCTGTTTCAGGCAGCTG. PCR conditions were 95 °C for 5 min, followed by 35 cycles of 95 °C for 30 s, T °C for 30 s (where T = 58 °C for exon 1 and 68 °C for exons 2–3), and 72 °C for 1 min, followed by 72 °C for 7 min. The PCR products were gel-purified (Qiagen) and sequenced directly using the following primers: for exon 1, 5′-TCCCTCTAACACATGACTCTG; for exons 2–3, 5′-TTGGATGGCACTGCGCGCTC, 5′-GCCAGGAGCGATGAACGCAAG, 5′-GAACAACGAGAAGGTGCTGGT, 5′-GCACCCAGCAGCCTTCGCTAA, 5′-TTAGCGAAGGCTGCTGGGTGC, and 5′-GCCTCTTGCGTTCATCGCTCCT.

ACKNOWLEDGMENTS. We thank Drs. Jurrien Dean (Eunice Kennedy Shriver National Institute of Child Health and Human Development), Lothar Hennighausen (National Institute of Diabetes and Digestive and Kidney Diseases), Toren Finkel (NHLBI), and Phil Gage (University of Michigan) for critical comments. Professional technical support for this study was provided in part by the personnel of the Pathology/Histotechnolgy Laboratory, Frederick National Laboratory for Cancer Research, and Leidos Biomedical Research Institute, Inc. This study was supported by the Divisions of Internal Research, NHLBI and National Eye Institute.

1. Gómez-Martín D, Díaz-Zamudio M, Galindo-Campos M, Alcocer-Varela J (2010) Early growth response transcription factors and the modulation of immune response: Implications towards autoimmunity. *Autoimmun Rev* 9:454–458.
2. Forsdyke DR (1985) cDNA cloning of mRNAS which increase rapidly in human lymphocytes cultured with concanavalin-A and cycloheximide. *Biochem Biophys Res Commun* 129:619–625.
3. Sukhatme VP, et al. (1988) A zinc finger-encoding gene coregulated with c-fos during growth and differentiation, and after cellular depolarization. *Cell* 53:37–43.
4. DeLigio JT, Zorio DA (2009) Early growth response 1 (EGR1): A gene with as many names as biological functions. *Cancer Biol Ther* 8:1889–1892.
5. Nguyen HQ, Hoffman-Liebermann B, Liebermann DA (1993) The zinc finger transcription factor Egr-1 is essential for and restricts differentiation along the macrophage lineage. *Cell* 72:197–209.
6. Suva LJ, Ernst M, Rodan GA (1991) Retinoic acid increases zif268 early gene expression in rat preosteoblastic cells. *Mol Cell Biol* 11:2503–2510.
7. Huang RP, et al. (1997) Decreased Egr-1 expression in human, mouse and rat mammary cells and tissues correlates with tumor formation. *Int J Cancer* 72:102–109.
8. Baron V, Adamson ED, Calogero A, Ragona G, Mercola D (2006) The transcription factor Egr1 is a direct regulator of multiple tumor suppressors including TGFbeta1, PTEN, p53, and fibronectin. *Cancer Gene Ther* 13:115–124.
9. Joslin JM, et al. (2007) Haploinsufficiency of EGR1, a candidate gene in the del(5q), leads to the development of myeloid disorders. *Blood* 110:719–726.
10. Davis S, Bozon B, Laroche S (2003) How necessary is the activation of the immediate early gene zif268 in synaptic plasticity and learning? *Behav Brain Res* 142:17–30.
11. Knapska E, Kaczmarek L (2004) A gene for neuronal plasticity in the mammalian brain: Zif268/Egr-1/NGFI-A/Krox-24/TIS8/ZENK? *Prog Neurobiol* 74:183–211.
12. Bettini M, Xi H, Milbrandt J, Kersh GJ (2002) Thymocyte development in early growth response gene 1-deficient mice. *J Immunol* 169:1713–1720.
13. Collins S, et al. (2008) Opposing regulation of T cell function by Egr-1/NAB2 and Egr-2/Egr-3. *Eur J Immunol* 38:528–536.
14. Du N, et al. (2014) EGR2 is critical for peripheral naïve T-cell differentiation and the T-cell response to influenza. *Proc Natl Acad Sci USA* 111:16484–16489.
15. Findlater GS, McDougall RD, Kaufman MH (1993) Eyelid development, fusion and subsequent reopening in the mouse. *J Anat* 183:121–129.
16. Li C, Guo H, Xu X, Weinberg W, Deng CX (2001) Fibroblast growth factor receptor 2 (Fgfr2) plays an important role in eyelid and skin formation and patterning. *Dev Dyn* 222:471–483.
17. Shi F, et al. (2013) The expression of Pax6 variants is subject to posttranscriptional regulation in the developing mouse eyelid. *PLoS One* 8:e53919.
18. Gregory-Evans CY, Williams MJ, Halford S, Gregory-Evans K (2004) Ocular coloboma: A reassessment in the age of molecular neuroscience. *J Med Genet* 41:881–891.
19. Herwig MC, et al. (2011) Preterm diagnosis of choristoma and choroidal coloboma in Goldenhar's syndrome. *Pediatr Dev Pathol* 14:322–326.
20. Trivedi N, Nehete G (2013) Complex limbal choristoma in linear nevus sebaceous syndrome managed with scleral grafting. *Indian J Ophthalmol* 64:692–694.
21. Nakao S, et al. (2007) Dexamethasone inhibits interleukin-1beta-induced corneal neovascularization: Role of nuclear factor-kappaB-activated stromal cells in inflammatory angiogenesis. *Am J Pathol* 171:1058–1065.
22. Graw J (2003) The genetic and molecular basis of congenital eye defects. *Nat Rev Genet* 4:876–888.
23. Graw J (2009) Genetics of crystallins: Cataract and beyond. *Exp Eye Res* 88:173–189.
24. Tong L, et al. (2006) Expression and regulation of cornified envelope proteins in human corneal epithelium. *Invest Ophthalmol Vis Sci* 47:1938–1946.
25. Chaerkady R, et al. (2013) The keratoconus corneal proteome: Loss of epithelial integrity and stromal degeneration. *J Proteomics* 87:122–131.
26. Libby RT, et al. (2003) Modification of ocular defects in mouse developmental glaucoma models by tyrosinase. *Science* 299:1578–1581.
27. Graw J (2010) Eye development. *Curr Top Dev Biol* 90:343–386.
28. Chow RL, Lang RA (2001) Early eye development in vertebrates. *Annu Rev Cell Dev Biol* 17:255–296.
29. Fischer AJ, McGuire JJ, Schaeffel F, Stell WK (1999) Light- and focus-dependent expression of the transcription factor ZENK in the chick retina. *Nat Neurosci* 2:706–712.
30. Bitzer M, Schaeffel F (2002) Defocus-induced changes in ZENK expression in the chicken retina. *Invest Ophthalmol Vis Sci* 43:246–252.
31. Schippert R, Burkhardt E, Feldkaemper M, Schaeffel F (2007) Relative axial myopia in Egr-1 (ZENK) knockout mice. *Invest Ophthalmol Vis Sci* 48:11–17.
32. Li T, et al. (2008) Evaluation of EGR1 as a candidate gene for high myopia. *Mol Vis* 14:1309–1312.
33. Hu CY, et al. (2006) Egr1 gene knockdown affects embryonic ocular development in zebrafish. *Mol Vis* 12:1250–1258.
34. Zhang L, et al. (2003) A role for MEK kinase 1 in TGF-beta/activin-induced epithelium movement and embryonic eyelid closure. *EMBO J* 22:4443–4454.
35. Bhattacharyya S, et al. (2008) Smad-independent transforming growth factor-beta regulation of early growth response-1 and sustained expression in fibrosis: Implications for scleroderma. *Am J Pathol* 173:1085–1099.
36. Oka M, Kudo H, Sugama N, Asami Y, Takehana M (2008) The function of filensin and phakinin in lens transparency. *Mol Vis* 14:815–822.
37. Shiels A, Bassnett S (1996) Mutations in the founder of the MIP gene family underlie cataract development in the mouse. *Nat Genet* 12:212–215.
38. Michea LF, Andrinolo D, Ceppi H, Lagos N (1995) Biochemical evidence for adhesion-promoting role of major intrinsic protein isolated from both normal and cataractous human lenses. *Exp Eye Res* 61:293–301.
39. Steele EC, Jr, et al. (1997) Identification of a mutation in the MP19 gene, Lim2, in the cataractous mouse mutant To3. *Mol Vis* 3:5.
40. Gong X, Agopian K, Kumar NM, Gilula NB (1999) Genetic factors influence cataract formation in alpha 3 connexin knockout mice. *Dev Genet* 24:27–32.
41. Maggs DJ, Miller PE, Orfi O (2008) Slatter's Fundamentals of Veterinary Ophthalmology (Elsevier Inc., Amsterdam), 4th Ed, p 108.
42. Beermann F, Orlow SJ, Lamoreux ML (2004) The Tyr (albino) locus of the laboratory mouse. Mamm Genome 15:749–758.
43. Lee SL, Tourtellotte LC, Wesselschmidt RL, Milbrandt J (1995) Growth and differentiation proceeds normally in cells deficient in the immediate early gene NGFI-A. *J Biol Chem* 270:9971–9977.